Cerebral Cortex December 2015;25:4667–4677
doi:10.1093/cercor/bhu148
Advance Access publication July 1, 2014

Task Dependence, Tissue Specificity, and Spatial Distribution of Widespread Activations in Large Single-Subject Functional MRI Datasets at 7T

Javier Gonzalez-Castillo[1], Colin W. Hoy[1], Daniel A. Handwerker[1], Vinai Roopchansingh[2], Souheil J. Inati[2], Ziad S. Saad[3], Robert W. Cox[3] and Peter A. Bandettini[1,2]

[1]Section on Functional Imaging Methods, Laboratory of Brain and Cognition, [2]Functional MRI Facility and [3]Scientific and Statistical Computing Core, National Institute of Mental Health, National Institutes of Health, Bethesda, MD 20892, USA

Address correspondence to Dr Javier Gonzalez-Castillo. Email: javier.gonzalez-castillo@nih.gov

It was recently shown that when large amounts of task-based blood oxygen level–dependent (BOLD) data are combined to increase contrast- and temporal signal-to-noise ratios, the majority of the brain shows significant hemodynamic responses time-locked with the experimental paradigm. Here, we investigate the biological significance of such widespread activations. First, the relationship between activation extent and task demands was investigated by varying cognitive load across participants. Second, the tissue specificity of responses was probed using the better BOLD signal localization capabilities of a 7T scanner. Finally, the spatial distribution of 3 primary response types—namely positively sustained (pSUS), negatively sustained (nSUS), and transient—was evaluated using a newly defined voxel-wise waveshape index that permits separation of responses based on their temporal signature. About 86% of gray matter (GM) became significantly active when all data entered the analysis for the most complex task. Activation extent scaled with task load and largely followed the GM contour. The most common response type was nSUS BOLD, irrespective of the task. Our results suggest that widespread activations associated with extremely large single-subject functional magnetic resonance imaging datasets can provide valuable information about the functional organization of the brain that goes undetected in smaller sample sizes.

Keywords: activation extent, negative BOLD, single subject, transients

Introduction

In a previous study (Gonzalez-Castillo et al. 2012), we showed that it is possible to detect blood oxygen level–dependent (BOLD) signal fluctuations time-locked with the experimental paradigm in the majority of the brain at the single-subject level, using a simple visual stimulation plus attention control task and approximately 500 min of functional data per subject. Detected individual voxel-wise responses followed 3 primary patterns: positive responses sustained for the duration of the task, negative responses sustained for duration of the task, and transient responses present only at task onsets/offsets. Concurrently, using a group analysis approach, Thyreau et al. (2012) found that, when combining data from 1326 subjects, statistically significant activations in response to passive viewing of faces covered the majority of the brain. These 2 studies pose challenging questions regarding functional localization and the relationship between statistical and biological significance in larger-than-usual functional magnetic resonance imaging (fMRI) datasets. Importantly, these interpretational challenges may soon not be specific to large fMRI datasets, but of relevance to most fMRI studies as improvements in fMRI hardware and methodology keep translating into substantial increases in temporal and contrast signal-to-noise ratios for individual scans (Triantafyllou et al. 2005).

With respect to statistical versus biological significance, both studies interpreted their results differently. Thyreau et al. (2012) concluded that classical statistical univariate analyses produce less anatomically relevant results (white matter [WM] activations) as subject count increases. In the case of Gonzalez-Castillo et al. (2012), the authors evaluated biological significance by studying whether or not the spatial distribution of whole-brain responses was meaningful. Clustering of whole-brain voxel-wise hemodynamic responses resulted in anatomically and functionally meaningful parcellations that were symmetric across hemispheres and reproducible across subjects. Based on these results, the authors concluded that, although a neuronal origin for all response shapes could not be determined, detected responses seemed to be biologically significant in the same way that resting-state patterns of BOLD signal fluctuations have proven to be biologically significant in resting-state fMRI (Smith et al. 2009).

To further advance our understanding of the biological significance of widespread BOLD activations in large fMRI datasets, we acquired 100 functional runs in each of 3 subjects. Stimulation and cognitive load were varied across subjects to evaluate how task load affects activation extent in large single-subject fMRI datasets. In particular, one subject performed a letter/number discrimination task superimposed on a full field-of-view (FOV) flickering checkerboard (same task as in Gonzalez-Castillo et al. (2012)); a second subject had to simply fixate on the center of a full FOV flickering checkerboard; and a third subject only received visual stimulation (i.e., flickering checkerboard) in the left hemifield of the FOV while fixating. To minimize partial volume effects (a potential limitation of Gonzalez-Castillo et al.), data were acquired using a 7T system and voxels 6.7 times smaller than in the original study (Gonzalez-Castillo et al. 2012). The lower sensitivity to large veins and the smaller BOLD point spread function at higher magnetic fields (Shmuel et al. 2007) additionally contribute to the increase in spatial specificity of responses in this second dataset. We computed activation maps for all tasks using an increasing number of functional runs (N_{runs}) ranging from 1 to 100 in intervals of 5. At each N_{runs} level, we computed activation maps and the percentage of significantly active gray matter (GM) voxels. For the subject performing the original visual stimulation plus attention control task, voxels with BOLD signals time-locked with the task account for 86% of GM. When task load was modulated by removing the attention control component of the task or changing the stimulation FOV, activation extent shows a positive correlation with task load independently of how many functional scans (N_{runs}) enter the analysis. This suggests a biological significance for the detected responses. In addition to activation extent, we also evaluated how the spatial distribution of response shapes varied

across experimental conditions. Our results highlight how positively sustained (pSUS) responses—those commonly reported in fMRI—account for fewer than half of all significantly active voxels irrespective of the task. This result suggests that transients and negatively sustained (nSUS) responses need to be studied in more detail to obtain a complete picture of how the brain reacts to external task demands. To appropriately discuss the new results within the context of our original observation of widespread activations (Gonzalez-Castillo et al. 2012), all new analyses were conducted both on the newly acquired 7T dataset and on the original 3T data. Moreover, in order to better interpret differences across both datasets, a series of data-quality metrics—namely spatial smoothness, temporal signal-to-noise ratio (TSNR) and contrast-to-noise ratio (CNR)—were computed and are reported in the Results section.

Materials and Methods

Subjects

Three subjects with no known history of neurological disorders (2 females; age = 25 ± 2.5 years) completed this study. All participants gave informed consent in compliance with a protocol approved by the Institutional Review Board of the National Institute of Mental Health in Bethesda, MD, USA.

Experimental Tasks

All functional runs had the same organization of blocks. An initial 10-s rest period was followed by 5 repetitions of a 20-s task block and a 40-s rest block. An additional 10 s of rest were added at the end of each functional run, resulting in 320 s runs. During the rest periods, subjects were instructed to remain still and focus their attention on a black fixation crosshair over a gray background. Note that the paradigm from our prior study at 3T had an additional 20 s of rest at the beginning of each run and used a white fixation cross on a black background. During the task epochs, each subject did 1 of 3 different tasks described below. Each subject always performed the same task across all 100 runs.

1. *Full Field-of-View Visual Stimulation + Attention Control Task* (*fFOV + Task*): The subject was instructed to focus his/her attention on a crosshair at the center of a full FOV flickering checkerboard (frequency = 8 Hz) and to perform a letter/number discrimination task. Four random alphanumeric characters appeared for 400 ms at random intervals in the center of the flickering checkerboard during each block. The subject was provided with a four-button response box in his/her right hand and was instructed to press one button if the character on the screen was a letter and another button if it was a number (same as in Gonzalez-Castillo et al. (2012)).
2. *Full Field-of-View Visual Stimulation Only* (*fFOV Only*): The subject was instructed to focus his/her attention on a crosshair in the center of a full FOV flickering checkerboard (frequency = 8 Hz). No letter/number discrimination task was present.
3. *Hemifield Visual Stimulation* (*hFOV Only*): The subject was instructed to focus his/her attention on a crosshair in the center of a left hemifield flickering checkerboard (frequency = 8 Hz; degrees left of center = 3). No letter/number discrimination task was present.

Data Acquisition

Imaging was performed on a Siemens 7T MRI scanner equipped with a 32-element receive coil (Nova Medical, Wilmington, MA, USA). Functional runs were obtained using a gradient-recalled, single-shot, echo-planar imaging (EPI) sequence (TR = 2.0 s, TE = 25 ms, FA = 50°, 54 oblique slices, slice thickness = 2 mm, spacing = 0 mm, in-plane resolution = 2 × 2 mm, FOV = 192 mm, acceleration factor (GRAPPA) = 2). T_1-weighted magnetization-prepared rapid gradient-echo data were also acquired for presentation and alignment purposes (sagittal prescription, number of slices per slab = 192, slice thickness = 1 mm, square FOV = 256 mm, image matrix = 256 × 256). Acquisition of the entire dataset required an average of 11 visits per subject.

Data from the previous study were collected on a General Electric (GE) 3T MRI scanner with relatively minor differences in echo-planar and structural scans, most notably in resolution (3.75 × 3.75 × 3.8 and 0.94 × 0.94 × 1.2 mm, respectively) and flip angle (75° in functional runs). See Gonzalez-Castillo et al. (2012) for additional details.

Data Preprocessing

The Analysis of Functional NeuroImages (AFNI) software (Cox 1996) was used for data preprocessing. For individual EPI runs, preprocessing included: 1) discarding initial 4 volumes to allow magnetization to reach steady-state; 2) slice-timing correction; 3) intrarun motion correction; 4) within-subject interrun spatial co-registration; 5) removal of signal changes proportional to motion parameters and their first derivatives; and 6) intensity normalization, by dividing each time-series by its own mean. The only difference in preprocessing between studies is the lack of physiological noise correction in the new study due to non-availability of respiratory and cardiac traces. No additional spatial smoothing was performed as part of the preprocessing.

For each EPI run, an intracranial voxel mask was generated using the *3dAutomask* program in AFNI. These masks were combined into a single mask at the subject level. The resulting masks were used in subsequent analyses to restrict computations only to voxels for which BOLD data are available for all 100 runs. This method compensates for small differences in imaged FOV across scanner visits. Additionally, voxels with high variance were removed from the mask. High-variance voxels were defined separately for each subject as those with a temporal standard deviation of the residuals for the SUS model (see model definition below) >10 in 1 or more runs. This resulted in the removal of a small number of voxels per subject located either at the edges of the brain or overlapping vasculature.

Additionally, GM and WM masks were generated using the segmentation algorithm available in SPM8 (http://www.fil.ion.ucl.ac.uk/spm/) and constrained to the intracranial masks. WM masks were then further restricted by eroding the outer most layer of voxels with the *3dmask_tool* AFNI program.

Statistical Analyses/Activation Extent

Statistical analyses were performed using an increasing number of runs (N_{runs}) ranging from 1 to 100 in steps of 5. To minimize any bias in the estimates of activation extent, 10 random permutations per N_{runs} level were used, with the exception of $N_{runs} = 100$ for which only a single case could be computed. For $N_{runs} = 1$, 10 runs were randomly selected for each subject.

All statistical analyses were conducted with the AFNI program *3dREMLfit*, which accounts for temporal autocorrelation in the noise of functional MRI (fMRI) time-series using an ARMA (1, 1) model. The statistical analyses were performed using 3 different models for the predicted BOLD response:

1. *Sustained-Only Response Model* (*SUS*): Here, the expected BOLD response associated with the task was modeled via convolution of a gamma-variate function (Cohen 1997) with a boxcar function that matches the experimental paradigm (i.e., "1s" during active blocks and "0s" during rest/fixation blocks). This case corresponds to the most conventional approach to the analysis of block fMRI data (Fig. 1*A*).
2. *Onset + Sustained + Offset Response Model* (*OSO*): Here, in addition to the sustained response of the SUS model, 2 additional BOLD responses were included. First, a stimulus-onset BOLD response was modeled as the convolution of the same gamma-variate function with a boxcar function with ones only at active epoch onsets. Similarly, the stimulus-offset BOLD response was modeled by convolving the gamma-variate function with a boxcar function with ones only at active epoch offsets. This is equivalent to the method previously used by Uludag (2008) and a subset of the OSORU model proposed by Harms and Melcher (2003) (Fig. 1*B*).
3. *Unconstrained Shape Response Model* (*UNC*): Here, no *a priori* information on the shape of the BOLD response is included other

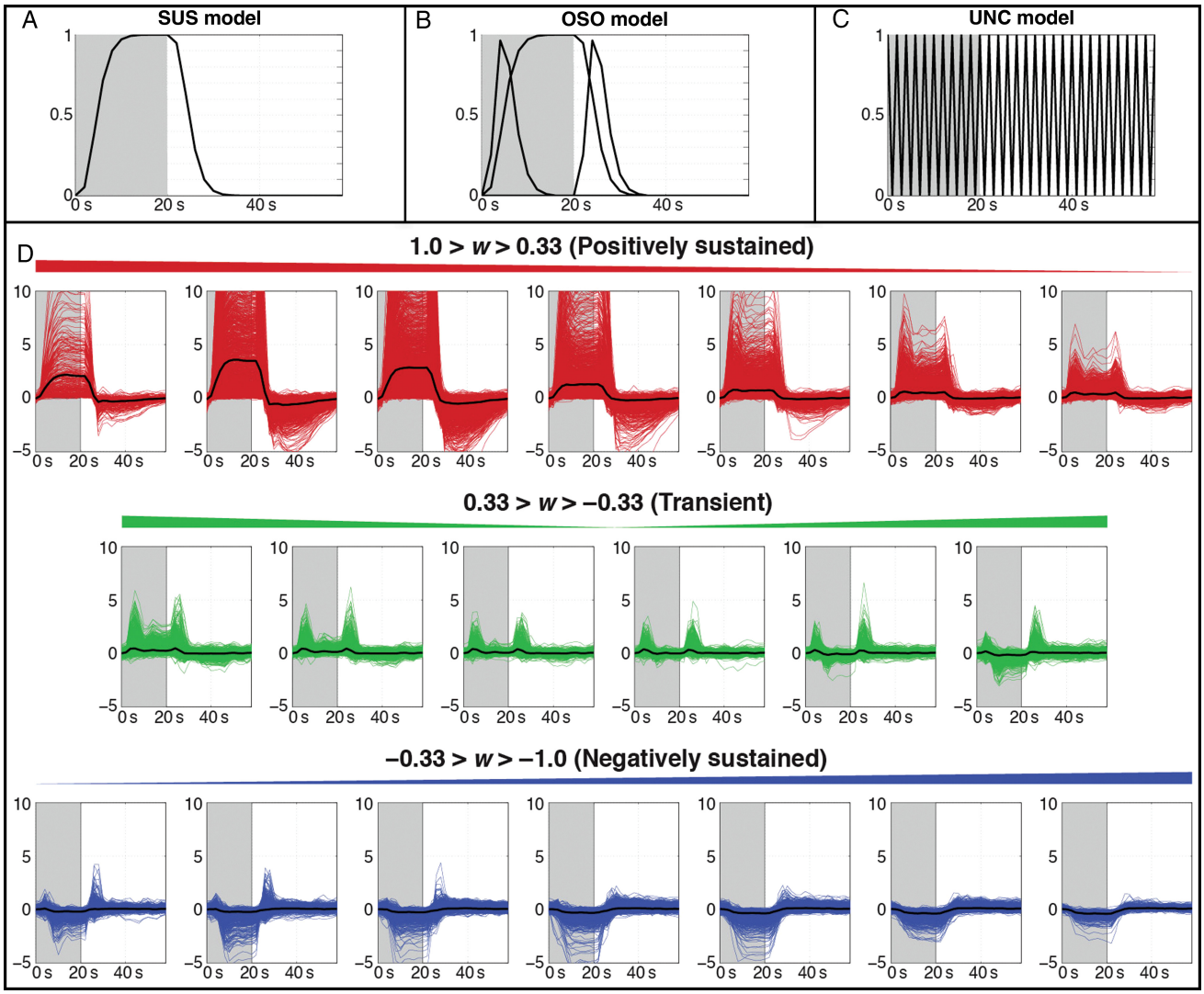

Figure 1. (*A–C*) Response models for 1 cycle (60 s) of the experimental paradigm, with task blocks (20 s) colored in gray. (*A*) The sustained (SUS) model consists of a gamma-variate BOLD response during the task block. (*B*) The onset + sustained + offset (OSO) model adds transient responses at the onset and offset of the task block to the SUS model. (*C*) The unconstrained (UNC) model uses finite impulse response (FIR) functions to model the data with no *a priori* information beyond task timing. (*D*) Categorization of response types in active GM for the 7T fFOV + Task subject. Impulse response functions estimated using the UNC model are separated into 20 bins according to the waveshape index (w) and classified as positively sustained (red), transient (green), or negatively sustained (blue). The mean response from within each bin is overlaid in black.

than the cyclic nature of the experimental paradigm. Therefore, the reference BOLD response function here consisted of a set of 30 impulse functions centered at acquisition times spanning the duration of one task cycle (20 s task + 40 s rest) (Fig. 1*C*).

In all instances, maps of significant activation were computed for the overall model (F-stat) using a voxel-wise false-discovery rate (FDR)-corrected statistical threshold of $p_{FDR} < 0.05$ (AFNI program *3dFDR*).

Modified Waveshape Index

Harms and Melcher (2003) previously defined a metric called a waveshape index that was capable of distinguishing between sustained and transient responses. This index permits both looking at the spatial distribution of these 2 types of responses as well as sorting voxel-wise responses in terms of their "sustained-like" and "transient-like" characteristics. As originally devised, the index does not distinguish between pSUS and nSUS responses. Given that our interest lies in evaluating these 2 types of responses separately, we defined a modified version of the waveshape index based on the OSO model described above as follows:

$$w = \frac{\beta_{SUS}}{|\beta_{SUS}| + |\beta_{ON}| + |\beta_{OFF}|} \quad (1)$$

where β_{SUS} is the effect size for the sustained response, β_{ON} is the effect size for the onset response, and β_{OFF} is the effect size for the offset response, all according to the fits to the basis functions in the OSO model at $N_{runs} = 100$. When defined this way, the waveshape index (w), ranges from −1 to 1, with $w = -1$ indicating purely nSUS responses, $w = 1$ indicating purely pSUS responses, and transient response shapes corresponding to w in the vicinity of zero. Note that combining the magnitudes of the onset and offset components does not allow w to differentiate between positive and negative transients or onset and offset responses. All transients were grouped together in this way to better compare transient-like and sustained-like responses. Also, notice that the intensity normalization step, performed as part of preprocessing, does not alter the sign of the beta weights that constitute the input to this waveshape analysis because the voxel-wise mean is always a positive value.

Voxels were discretely categorized according to response type by dividing the range of w into thirds, such that responses with $w < -0.33$ were labeled as nSUS, responses with $-0.33 < w < 0.33$ were labeled as transient, and responses with $w > 0.33$ were labeled as pSUS. Figure 1*D* assesses the validity of the index as a means to classify voxel-wise BOLD responses by showing the impulse response functions output by the UNC model for each statistically significant voxel in GM for the 7T "fFOV + Task" subject as a function of w. Responses were grouped into 20 bins. Responses in bins corresponding to pSUS responses are presented in red, transient responses in green, and nSUS responses in blue. The mean response from each bin is overlaid in black. Figure 1*D* shows that w grouped voxel-wise responses according to shape as expected.

To evaluate the spatial distribution of the 3 response types, waveshape maps were generated for all subjects (Fig. 4). To evaluate the contribution of each response type to overall activation extent in GM, histograms of w across GM voxels were computed for each subject (Fig. 6*B*). The proportions of each response type within active GM for a given subject and ratios between those proportions were also calculated (Fig. 6*C*).

Effect Size Analysis

Finally, in order to evaluate potential systematic differences in effect size across response types, the magnitudes of pSUS, nSUS, and transient responses were compared (Fig. 6*A*). For this purpose, an average effect size per response type and subject was computed using only the top 5% voxels with the strongest response within each response category. For sustained responses (both pSUS and nSUS), response magnitude is reported in terms of the beta coefficient for the sustained component of the OSO model (β_{SUS}). For transient responses, we used the average of the beta coefficients for the onset (β_{on}) and the offset (β_{off}) responses. Results from this part of the analysis are reported in Table 3.

Data-Quality Metrics

Spatial Smoothness

The spatial smoothness of the EPI data was estimated using AFNI program *3dFWHMx,* restricting the estimation only to voxels within each subject's intracranial voxel mask.

Temporal Signal-to-Noise Ratio

TSNR is commonly defined on a voxel-wise manner as the ratio of the mean across time divided by the standard deviation across time. We report TSNR as the average TSNR across all voxels in the WM mask described above. This was done to avoid bias by large responses in active GM voxels.

Contrast-to-Noise Ratio

CNR is defined here as the ratio of the effect size for the sustained model (β_{SUS} from the SUS model) to the temporal standard deviation of the residuals. To avoid any bias due to outliers, CNR is computed for all voxels within a 5-mm radius Region of Interest centered at the peak voxel within right primary visual cortex. Right primary visual cortex was defined as the union of the right lingual gyrus and the right calcarine gyrus of the MNI macrolabel atlas distributed with AFNI.

Results

Behavioral Results

Behavioral data were only collected for 1 subject, as the other 2 were asked to passively look at the screen where the stimuli were being projected. For this subject, average accuracy across runs was 97 ± 3.5%. Minimum accuracy was 90%. For the other 2 subjects, we visually inspected time-series to ensure that the 5 pertinent blocks of activation were present. If one or more blocks were not present, the run was discarded. A total of 100 good runs were obtained in each of the 3 subjects.

Table 1
Comparison of data-quality metrics across experiments

	Smoothness (mm)	White matter TSNR	Visual cortex CNR
3T	6.55 ± 0.07	349 ± 19	5.17 ± 0.65
7T	2.38 ± 0.10	106 ± 12	4.36 ± 0.82
3T/7T	2.76	3.30	1.18

Single run metrics were averaged across all 100 runs. Values averaged across the 3 subjects are shown with standard deviations.

Data-Quality Comparison Across Studies

Given differences in field strength, vendor, and acquisition parameters across the datasets (e.g., 3T and 7T data), we computed a series of quality metrics to better understand these differences during the interpretation of the results. Each metric was computed individually for each run. Averages across all runs from all subjects are reported on Table 1. This table shows how estimated spatial smoothness was 2.76 times higher for the 3T data; TSNR was 3.30 times bigger for the 3T data; and CNR was 1.18 times bigger for the 3T data when compared with the 7T data.

Activation Extent Results

Figure 2 shows percent of active GM voxels as a function of N_{runs} for both the current and prior study. Activation extent significantly increased with N_{runs} for all tasks and models in the new experiments reported here. Percentage of active GM at $N_{runs} = 1$ and $N_{runs} = 100$ for all models in all 7T conditions, as well as the average values across the 3T subjects, are reported in Table 2. For the fFOV + Task condition at 7T, GM activation extent reached 86% for the OSO model at $N_{runs} = 100$. Although lower than the GM activation extent for the original 3T dataset (96%), the new experimental setup still produced significant activations spread all over the brain and well beyond areas commonly considered to have a primary relationship with the task (Fig. 3). This happened despite differences in voxel size, inherent spatial smoothness, TSNR and CNR between both datasets.

To test the biological significance of responses, task load was modulated across subjects in the new experiments. For all models and all N_{runs} levels, task load modulated activation extent (Fig. 2). In particular, the simpler the task, the lower the activation extent reported independently of the response model and N_{runs}.

Activation maps in Figure 3 illustrate the spread of activity from $N_{runs} = 1$ to 100 for all 7T (voxel size = 8 mm^3) subjects and one representative 3T (voxel size = 53.4 mm^3) subject across all response models. For all subjects and models, activation at $N_{runs} = 100$ expanded beyond primary sensory/motor regions; still, the extent of significant activations was reduced for subjects with lower task demands. This was particularly true for the hemifield stimulation condition, for which large portions of ipsilateral cortex remained nonsignificant at $N_{runs} = 100$. Nevertheless, even for this condition, activation extent still reached 44% of GM volume for the OSO model and extended well beyond contralateral visual cortex.

Finally, active areas in the 7T maps generally tended to follow the GM contour more closely than in the 3T maps for both $N_{runs} = 1$ and $N_{runs} = 100$. However, significantly active WM voxels

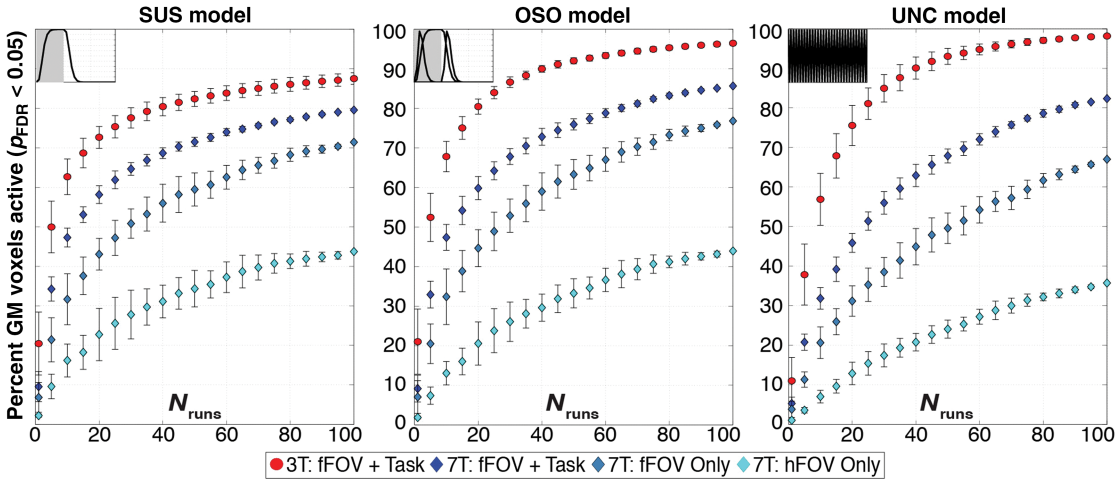

Figure 2. Evolution of activation extent in GM as a function of runs entering the analysis (N_{runs}) for both the 3T and 7T data for $p_{FDR} < 0.05$. Each panel shows results for a different response model. Markers track expansion of GM activation as N_{runs} increases for averages of all 3T subjects (red), the same fFOV + Task condition at 7T (dark blue), "fFOV Only" (blue), and "hFOV Only" (light blue). Error bars for 3T data show standard deviation across subjects, while error bars for 7T data represent standard deviation across permutations within a single subject.

Table 2

Activation extent for $p_{FDR} < 0.05$ in GM compartment for all 3 models when: 1) only 1 run enters the analysis; and 2) 100 runs enter the analysis

B_0	Task	$N_{runs} = 1$			$N_{runs} = 100$		
		SUS	OSO	UNC	SUS	OSO	UNC
3T	fFOV + Task	20.5 ± 8.0%	21.0 ± 8.2%	11.0 ± 5.9%	87.5 ± 1.5%	96.4 ± 0.5%	98.2 ± 0.3%
7T	fFOV + Task	9.6 ± 3.8%	9.1 ± 3.4%	5.3 ± 1.6%	79.5%	85.6%	82.4%
	fFOV Only	6.9 ± 3.8%	7.0 ± 4.1%	3.8 ± 2.0%	71.4%	76.8%	67.0%
	hFOV Only	2.2 ± 0.4%	1.8 ± 0.4%	1.1 ± 0.2%	43.7%	43.9%	35.8%

Standard deviations were calculated across permutations within each subject for 7T data at $N_{runs} = 1$ and across permutations for all subjects for 3T data at both N_{runs} levels.

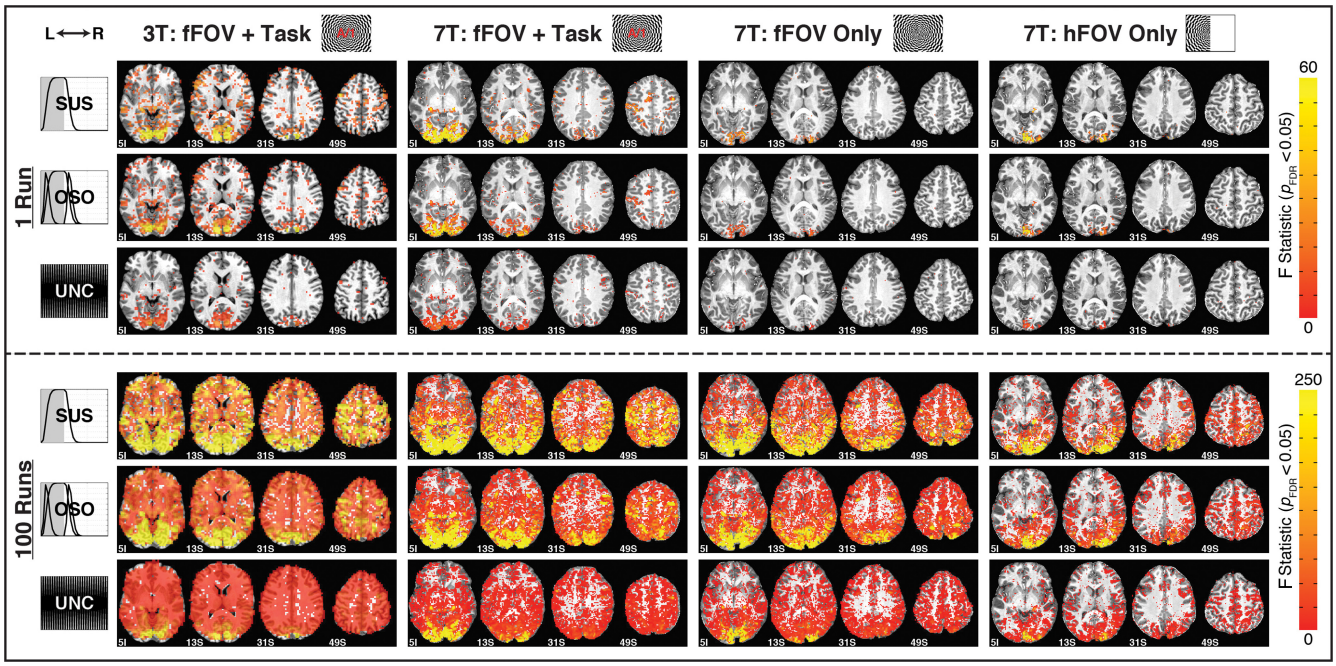

Figure 3. Maps of activation ($p_{FDR} < 0.05$) for $N_{runs} = 1$ (top 3 rows) and 100 (bottom 3 rows) across subjects and response models. Columns correspond to single subjects, and rows show results from different response models. The "SUS," "OSO," and "UNC" rows show significantly active F statistics for those models with yellow indicating stronger activation. Activation extent increases from $N_{runs} = 1$ to 100 and decreases from left to right due to differences in quality between 3T and 7T data and lower task demands in "fFOV Only" and "hFOV Only" conditions.

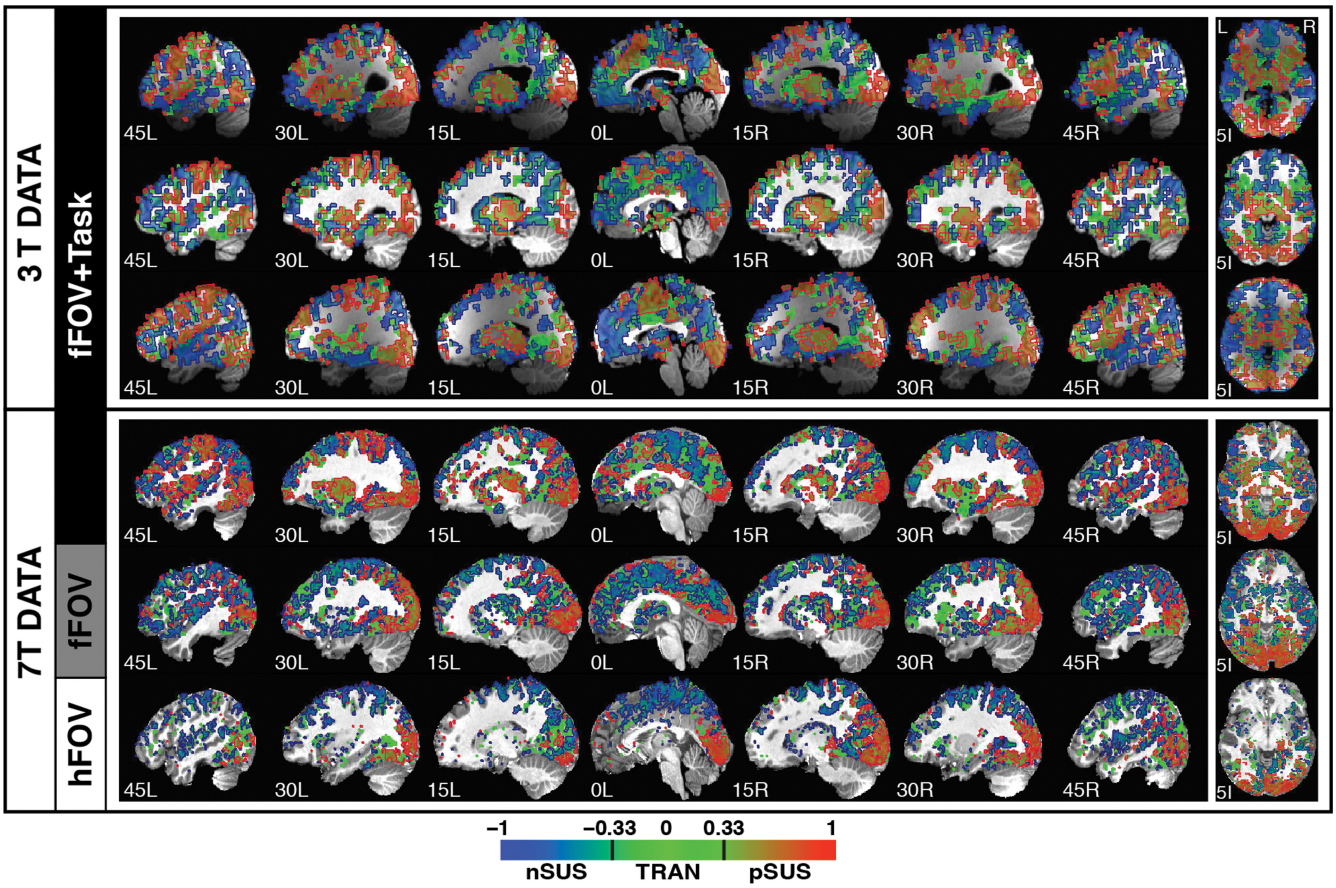

Figure 4. Spatial distribution of response types as categorized by the waveshape index (w) in a set of sagittal and axial slices for all 6 participants. A gradient scale was used to color each voxel according to its w index. Additionally, contours were overlaid in the map to depict the classification of voxels in 3 main primary response types: red = positively sustained responses ($0.33 < w < 1$); green = transient responses ($-0.33 < w < 0.33$); and blue = negatively sustained responses ($-1 < w < -0.33$).

were found covering large occipital regions at $N_{runs} = 100$ at 7T for both full FOV conditions (i.e., independently of whether or not the letter/number discrimination task was present).

Response-Type Contributions

Figure 4 shows the spatial distribution of pSUS (red), transient (green), and nSUS (blue) responses according to the waveshape index (w) for all significantly active voxels in GM in all 6 subjects (the 3 3T subjects acquired for the previous study (Gonzalez-Castillo et al. 2012) and the 3 7T subjects acquired as part of this study). The top 4 rows show subjects that were scanned under the fFOV + Task condition (top 3 rows correspond to the 3T subjects from the prior study). The 2 lower rows show the results for the 2 stimulation-only conditions acquired at 7T (fifth row shows the results for the "fFOV Only" condition and the sixth row for the "hFOV Only" case). Although intersubject variability in the spatial distribution of response types does exist across subjects, many important commonalities can be found. For example, in all 4 fFOV + Task subjects, pSUS responses cover large portions of bilateral occipital cortex, bilateral thalamus, bilateral inferior frontal cortex, as well as left primary and supplementary motor cortexes. Additionally, nSUS responses for these 4 subjects can be observed in right motor cortex, posterior cingulate cortex, anterior medial frontal cortex, bilateral precuneus, and portions of bilateral superior and medial temporal cortex. In addition, transient responses can be observed in all 6 subjects at the parieto-occipital junction.

Regarding the stimulation-only conditions, for the "fFOV Only" subject pSUS responses appear to be restricted mainly to bilateral occipital cortex and bilateral thalamus, although some additional small clusters with pSUS responses can be found in parietal and frontal cortex. In contrast, for the "hFOV Only" subject pSUS responses are constrained mainly to contralateral occipital cortex and lateral geniculate nucleus. Still, under the "hFOV Only" condition, there are some portions of the ipsilateral occipital cortex that responded in a pSUS manner. This is likely the result of the subject not maintaining consistent fixation across all runs. Nevertheless, the extent of pSUS activations in ipsilateral occipital cortex for this subject is much less than for the other 5 subjects.

Figure 5 shows the presence of transient-like responses (either by themselves or accompanied by some level of sustained-like response) for the 3 experimental conditions at 7T in all core regions of the task-set network (a limited set of regions that select and modulate downstream processes relevant to task performance) previously described by Dosenbach et al. (2006). In particular, for the 2 stimulation-only conditions (Fig. 5; upper 2 rows), pure transient responses can be observed in all 3 core regions—namely bilateral anterior insula/frontal operculum region (aI/fO) and the border of the dorsal anterior cingulate and medial superior frontal cortex (dACC/msFC). In

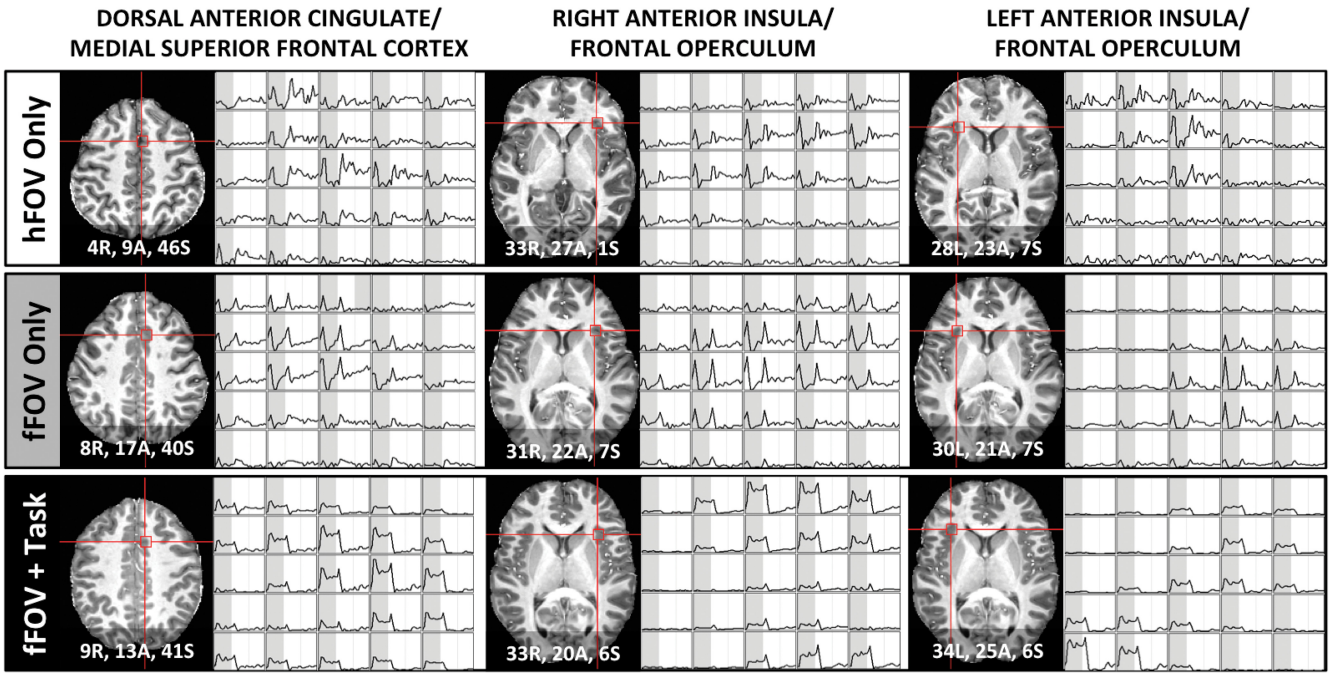

Figure 5. Voxel-wise responses for the 3 7T participants in the core regions of the task-set network (Dosenbach et al. 2006). The left-most column shows responses in a region at the border of the dorsal anterior cingulate and the medial superior frontal cortex. The middle and right-most columns show responses for voxels within the right and left anterior insula/frontal operculum, respectively. Coordinates provided in MNI space.

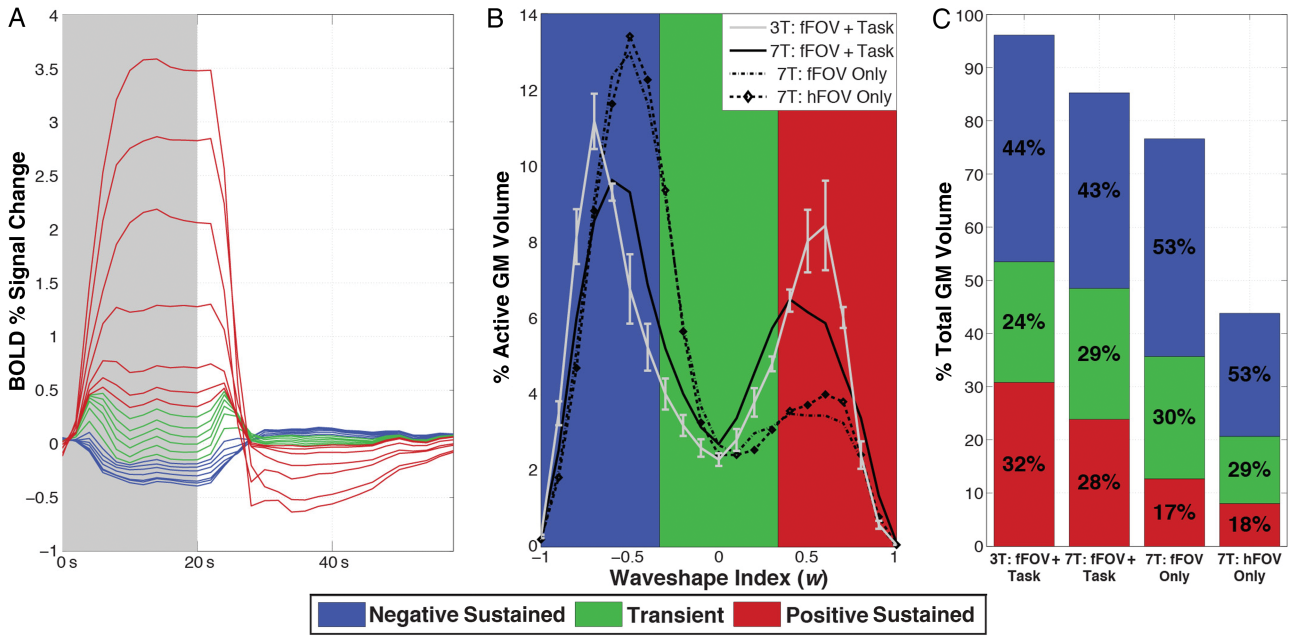

Figure 6. (*A*) Relative size of mean responses, as categorized by *w* into 20 bins in Figure 1*D*, for active GM voxels in the 7T fFOV + Task subject. Positively sustained, transient, and negatively sustained responses are colored in red, green, and blue, respectively. (*B*) Histograms of *w* as a percentage of active GM for each subject (average of 3T subjects shown with standard error bars), showing the relative abundance of each response type. (*C*) Bar graph showing contributions of each response type relative to total GM volume for all 7T and the average of the 3T subjects. The percentage of GM activation that each response type is responsible for in each subject is overlaid in black.

contrast, in the fFOV + Task condition, transient responses occur on top of pSUS responses (Fig. 5; bottom row).

Figure 6*A* shows the average hemodynamic response for the 7T fFOV + Task condition in each of the 20 bins used to evaluate the validity of the waveshape index (Fig. 1*D*). When overlapping these average response shapes on the same plot, it becomes apparent that pSUS responses are on average larger than transients and nSUS responses. Table 3 shows the relative size (as ratios) of the 3 responses types for all subjects. Independently of the experimental task under study, pSUS responses were substantially larger in magnitude than transient or nSUS responses. As for the relationship between transient

Table 3

Absolute value of ratios comparing the effect sizes of positively sustained (pSUS), negatively sustained (nSUS), and transient (Trans) response types, as categorized by w, at $N_{runs} = 100$

Scanner	Task	pSUS/nSUS	pSUS/Trans	nSUS/Trans
3T	fFOV + Task	3.19 ± 0.13	7.52 ± 1.28	2.37 ± 0.47
7T	fFOV + Task	8.01	6.96	0.87
	fFOV Only	8.67	8.05	0.93
	hFOV Only	9.17	8.11	0.88

Standard deviations calculated across subjects for 3T data.

Table 4

Ratio across hemispheres of the number of significant voxels with nSUS responses for the 2 visual stimulation-only conditions

Condition	Uncorrected R/L ratio	Corrected R/L ratio
7T: hFOV Only	1.43	1.47
7T: fFOV Only	0.88	0.90

The left columns show the ratio of significant nSUS voxels across hemispheres not taking into account differences in hemispheric sizes. The right column shows the same ratios after correcting for differences in the size of total GM masks across hemispheres.

and nSUS responses, a scanner dependence was observed with nSUS responses being approximately twice as big in magnitude as transient responses in the 3T data, but approximately equivalent in magnitude for the 7T data independently of the experimental condition.

Figure 6*B* shows histograms of w values across all significant GM voxels for all subjects. A bimodal distribution of response types can be observed for all subjects and conditions. For those performing the letter/number discrimination task the distributions are more heavily weighted towards the positive range of w compared with the other subjects. Figure 6*C* presents a summarized view of the histogram, where we only show the breakdown of the 3 categories as a percentage of active GM, relative to total GM volume. Independently of experimental condition, nSUS responses accounted for the largest proportion of active voxels in GM (over 40% in all cases, and over 50% in the cases where no letter/number discrimination task was performed). Transient responses account for approximately 30% of active GM voxels independently of task in the 7T data, though this proportion drops to an average of 24% in the 3T data. The proportion of pSUS responses is task dependent; they account for only ~18% of active GM in stimulation-only conditions; however, in subjects performing the letter/number discrimination task, the proportion of pSUS responses increased to surpass transients and account for ~30% of active GM (see Fig. 6*C*). Additionally, Table 4 shows the relative contributions of nSUS responses to GM activation across hemispheres both with and without correction for differences in hemispheric GM size. Regardless of whether or not the correction is applied, the computed ratios show how nSUS responses were heavily lateralized towards contralateral cortex during the "hFOV Only" condition; this strong asymmetry in spatial distribution dissipated for the "fFOV Only" condition.

Discussion

The results reported here represent an extension of previous studies aimed at better understanding the sensitivity limits of fMRI and the interpretational challenges associated with the detection of widespread activations in large fMRI datasets (Gonzalez-Castillo et al. 2012; Thyreau et al. 2012). Using a higher field system (7T > 3T) that produced images with higher nominal spatial resolution (3T/7T: 53/8 mm^3) and lower spatial smoothness (3T/7T: 6.55/2.38 mm) without incurring excessive losses in CNR (3T/7T: 5.17/4.36), we were able to confirm the presence of BOLD responses correlated with task-timing in over 86% of GM for a simple visual stimulation plus attention control task when compared with rest. Moreover, by modulating task demands across subjects, we showed that the extent of significant activations varies with task demands in large fMRI datasets in a manner similar to what it is commonly observed in regular size (2–5 functional runs per condition) fMRI studies. In particular, we showed that the lower the task demands, the lower the amount of GM voxels that become significantly active when 100 functional runs enter the analysis. Finally, we evaluated the relative contributions of unconventional response shapes—namely nSUS and transients—to activated regions. We now discuss some implications of these findings in further detail.

Statistical versus Biological Significance

The most common way to report task-based fMRI results is to generate statistical parametric maps (SPMs) under the assumption that there is a strong correlation between statistical and biological significance. To generate such maps, researchers must set a threshold criteria, which in fMRI is usually $p < 0.05$ corrected for multiple comparisons. This criteria is intended to minimize type I errors (false positives), but it translates into a substantial amount of type II errors (false negatives) (Lieberman and Cunningham 2009). This limitation becomes very apparent in large fMRI datasets where availability of additional data permits robust detection of a wider range of response shapes and magnitudes that otherwise remain statistically insignificant in smaller samples (Huettel and McCarthy 2001; Saad et al. 2003; Gonzalez-Castillo et al. 2012). The presence of these widespread activations in large datasets poses an important interpretational challenge and their biological and neuronal significance deserves additional attention.

Here, we extend our original work at 3T and provide evidence in support of a biological origin for widespread activations, as opposed to being simply the result of additional degrees of freedom or large acquisition voxels. First, we show that partial volume effects played a limited role in the original study, and that the original observation of widespread activation remains valid at a nominal spatial resolution approximately 7 times higher (3T/7T: 53/8 mm^3). Second, we show that activation extent is modulated by task demands in these large datasets in a similar manner to what happens in regular size fMRI datasets. Both results suggest that widespread activations, when present, do represent true task-driven alterations of the hemodynamic signal.

Nevertheless, it is worth noticing that increases in signal-to-noise in these 2 studies came at the cost of combining large amounts of data that were brought into a common space via spatial interpolation. Despite combining all necessary spatial transformations into a single interpolation step, this step will still introduce some level of artificial smoothness not present in the original raw data (Grootoonk et al. 2000). While such artificial smoothness cannot account for the observation of widespread activation across the whole brain (the smoothing kernel does not go beyond a few voxels), it will lead to an increase in

the observed percentage of active voxels (e.g., activation extent for a given location may leak into some neighboring voxels). In order to obtain a more accurate measure of exactly how much brain tissue gets modulated by an externally imposed task, it will be necessary not only to increase the nominal spatial resolution of the recordings (as done here) but, at the same time, also increase the signal-to-noise of each single measure. This goal may be achievable in the near future with the combination of additional increases in field strength, the use of more efficient receive coils, and improvements on the modeling of noise sources.

The remaining question—that of neuronal significance and interpretation—is more difficult. Given the range of response shapes and magnitudes that contribute to widespread fMRI activations, they most likely arise from a wide range of mechanisms and may represent a larger set of hemodynamic events and neuronal processes than those detectable with less data. This is particularly true in our experiments where the baseline condition (e.g., simple fixation) does not attempt to control for any specific cognitive process that accompany task performance (e.g., changes in arousal, attention, etc.). Key interpretational challenges within this framework include: differentiating task-essential regions (i.e., their processing capabilities are indispensable to the successful performance of the task) from task-accessory regions (i.e., those affected by task performance, but whose processing capabilities are not required for successful execution/perception of the task/stimulus); understanding how differences in baseline conditions affect the extent and distribution of these widespread responses (e.g., the use of more specific control conditions or combinations of them may help better separate the cognitive contributions of the different activation loci); discerning activations due to increased excitatory neuronal activity versus those due to increased inhibitory neuronal activity (see Logothetis (2008) for a discussion); and telling hemodynamic events tightly co-localized to neuronal activity apart from those that only manifest as a vascular-driven distant echo of true neuronal modulation at a different location. Addressing these interpretational challenges will not only require a better understanding of hemodynamic coupling mechanisms and embracing interregional hemodynamic variability (Chang et al. 2008; Handwerker et al. 2004) as a source of information instead of noise (see Orban et al. (2015)) for an elegant approach to extracting information from interregional variability), but will most likely necessitate the concurrent use of fMRI with other techniques such as electroencephalography, and transcranial magnetic stimulation. Here, as a simple initial step, we decided to group responses in 3 main categories—namely pSUS responses, nSUS responses, and transient responses—and to explore their spatial distribution and relative magnitudes in order to better understand their contribution to the overall observed activity.

Positively Sustained BOLD Responses

Positive BOLD signal deflections in response to task/stimulation are known to correlate well with local field potentials, suggesting positive BOLD is mainly determined by local processing of inputs to a given area (Goense and Logothetis 2008). Because of this deeper understanding, most of the time, pSUS responses constitute the only response type reported in task-based fMRI studies. Nonetheless, in the large datasets presented here, they account approximately for only one-third of active voxels in the fFOV + Task condition and less than one-fifth in the stimulation-only conditions (Fig. 6*C*). This suggests that any attempt to fully characterize the functional organization of the human brain with task-based fMRI cannot rely on reporting and interpreting only this type of response (Cauda et al. 2014).

Negatively Sustained BOLD Responses

Negative BOLD responses accounted for the largest percentage of active GM voxels irrespective of experimental condition. Although first regarded as a purely vascular effect (i.e., "blood stealing") (Harel et al. 2002), there is a growing consensus that sustained negative BOLD signals correspond mainly to inhibited regions (Saad et al. 2001; Shmuel et al. 2006; Devor et al. 2007), with the exception of negative BOLD in periventricular regions, which are suggested to arise from a purely vascular phenomena (Bianciardi et al. 2011). Assuming negative BOLD responses primarily indicate sites of neuronal inhibition, our results suggest neuronal inhibition is a widely distributed phenomena in the brain (it happens in over 21% of total GM for the "hFOV Only" condition, and over 35% of total GM in all other cases). Two additional trends were present in the data. First, higher task demands lead to a substantial increase in the volume occupied by nSUS BOLD responses. Second, there is a marked hemispheric asymmetry in the distribution of negative responses for the "hFOV Only" condition that disperses once both visual hemifields are stimulated (Table 4). These observations could be explained in terms of stronger fronto-parietal phase coupling contralateral to visual stimulation (Sauseng et al. 2005). Given the spread and distribution of negative BOLD foci, it would be difficult to explain these patterns of activation solely in terms of vascular territories (Tatu et al. 2012) and therefore attribute them to purely vascular or hemodynamic phenomena.

The magnitude of nSUS responses was substantially smaller (one-third or less; Fig. 6*A* and Table 3) than that of pSUS responses across all conditions. The lower effect sizes associated with negative BOLD relative to positive BOLD have been previously reported (Saad et al. 2001; Harel et al. 2002). Because of their lower magnitude, nSUS responses require larger datasets or higher signal-to-noise ratio to achieve appropriate detection. Still, these efforts are worthwhile. For example, Manson et al. (2008) used a sample of 56 multiple sclerosis patients and 60 age-matched controls to show that patients had significantly smaller negative BOLD responses in ipsilateral motor cortex during a simple visually cued hand movement task. According to the authors, insufficient inhibition of ipsilateral cortex, as indicated by decreased magnitude of negative BOLD responses, may help explain the impairments associated with the disease.

Transient BOLD Responses

Transient hemodynamic changes in response to long sustained stimulation have been previously reported for auditory (Harms and Melcher 2003), visual (Uludag 2008), somatosensory (Marxen et al. 2012), olfactory (Sobel et al. 2000), and higher order cognitive cortices (Dosenbach et al. 2006). Here, we show that, on average, these responses account for approximately 30% of active GM in the 3 experimental conditions tested at 7T. Moreover, we show that voxel-wise transient responses can occur both in isolation or in combination with both forms of sustained responses (Fig. 1*D*), which is also in agreement with the literature (Dosenbach et al. 2006; Petersen and Dubis 2012).

Though the spatial distribution of transient responses was quite variable across subjects (Fig. 5), some commonalities could still be found. For example, Figure 6 shows voxels in the dACC/msFC and aI/fO that responded at the onset and offset of the task across all 7T subjects. Dosenbach et al. (2006) hypothesized that these regions form a "core" system responsible for selecting and modulating downstream processing regions relevant to task performance for a large variety of tasks. The fFOV + Task condition required continuous performance of the attention task-set and elicited pSUS activity in addition to the transient responses in these regions, an activation pattern consistent with instantiation signals followed by maintenance of the task-set. In contrast, the "core" task-set regions showed only transient responses in the passively viewed, stimulation-only conditions. This result shows how working with large fMRI datasets permits detection of these "core" task-set regions by their differential responses to relatively low-level tasks, and in this way extends the findings in the original work of Dosenbach et al. (2006).

Differences Across Datasets

Two independent datasets acquired on different systems were used on this study. Key differences across datasets include field strength (3T vs. 7T), vendor (GE vs. Siemens) and nominal spatial resolution (53 vs. 8 mm^3). These factors translated into substantial differences in spatial smoothness and noise characteristics for the data.

With respect to spatial localization, BOLD fMRI data at 7T benefit from a lower contribution of intravascular signals due to a decreased T_2 of blood at this higher field (Yacoub et al. 2001; Duong et al. 2003). In addition, higher field strength allows us to reduce voxel size without incurring excessive losses in TSNR and CNR (see next paragraph). One additional factor affecting spatial resolution is how much the data are spatially smoothed in k-space prior to its transformation into image space. The 3T vendor uses a default filter for its data in k-space prior to reconstruction (Friedman et al. 2006). That is not the case for the 7T vendor. The combined effects of these 3 factors translated into an estimated spatial smoothing 2.76 times bigger on average for the 3T data when compared with the 7T data.

Regarding noise levels, TSNR and CNR estimates revealed that, for our particular scanning parameters, data acquired at the 7T system was noisier. Although higher field strength translates into higher signal levels, the use of smaller voxels causes the opposite effect. As a result of this, we observed an overall decrease in TSNR by a factor of 3.3 going from 3T to 7T. Nonetheless, smaller voxels helps alleviate partial volume effects in GM and translates into smaller losses in CNR (Newton et al. 2012). This phenomenon is clearly observable in our data, as CNR only decreased by a factor of 1.18 in the 7T data.

GM activation extent for the fFOV + Task condition decreased from 96% (3T) (Gonzalez-Castillo et al. 2012) to 86% (7T) across experiments. Moreover, significant activations at 3T covered large portions of WM, while at 7T active voxels remained primarily within the GM contour. These 2 observations can be explained by differences in signal-to-noise levels, differences in spatial specificity, or a combination of both. If lower signal-to-noise ratio is the primary contributor to these observations, one could expect activation area to keep increasing and possibly spread more into WM regions as more data become available. The potential additional presence of significant BOLD signal changes time-locked with the task in WM does not necessarily question the biological significance of our findings. Local hemodynamic changes that accompany metabolic demands are 2–3 times smaller in WM than in GM (Rostrup et al. 2000), making their detection more challenging. Moreover, BOLD activations have been previously reported in different sections of the corpus callosum in response to tasks with a heavy interhemispheric transfer component and that rely on callosal communication pathways (Tettamanti et al. 2002; Mazerolle et al. 2008; Gawryluk et al. 2011). It is feasible that BOLD activations in WM may provide important information about processing pathways in the brain. Still, our observation of significantly active voxels within WM ought to be interpreted with much care. As previously stated, increases in signal-to-noise ratio via averaging also come accompanied by artificial increases in spatial smoothness that can produce leakage of task-locked fluctuations from GM voxels into neighboring WM voxels. Moreover, the increase in nominal spatial resolution across studies heavily reduced the amount of significantly active voxels in WM. To more clearly address the issue of WM BOLD activations, further research is necessary to get a better understanding of the biological processes that can lead to local BOLD signal changes in pure WM voxels.

A second, alternative explanation for the decrease in active area across studies for the fFOV + Task condition could be the difference in spatial resolution and smoothness. If this were the main cause, one would expect to see additional reductions in active area for data of equivalent signal-to-noise characteristics acquired at much higher spatial resolutions. New technological advances will very likely permit acquisition of such data in the near future. In the meantime, it is difficult to accurately estimate the true level of sparsity for fMRI activations in response to externally driven tasks given the interactions described above. Nevertheless, it is worth noticing that a substantial increase in spatial resolution that came accompanied by losses in both CNR and TSNR only caused a small decrease in activation extent. We believe this result suggests that BOLD signal changes time-locked with experimental paradigms should be expected in larger portions of the brain than previously thought, even for the simplest of tasks.

Conclusions

The results presented here constitute additional evidence in support of a biological significance, as opposed to merely statistical significance, for widespread BOLD activations in larger-than-usual fMRI datasets. In particular, we show: 1) that significantly active voxels for a simple visual stimulation plus attention control task still cover the majority of GM (86%), despite data being acquired at a nominal resolution almost 7 times higher and concurrent losses in TSNR and CNR; 2) that activation extent and location varies with task demands in larger-than-usual datasets in a manner similar to how it does in common size datasets; 3) that nSUS responses account for the largest percentage of active GM voxels irrespective of task; and 4) that pSUS responses—those commonly reported in the literature—only accounted for one-third to one-fifth of active GM voxels depending on task demands. Overall, these results confirm the previous observation that BOLD activations are present in a larger set of brain regions than is commonly reported, highlight the informative value of reporting responses

other than pSUS, and refine some new interpretational challenges associated with the detection of widespread activations.

Funding

This research was supported by the Intramural Research Program of the National Institute of Mental Health (NIMH) at the National Institutes of Health (NIH).

Notes

Portions of this study utilized the high-performance computational capabilities of the Biowulf Linux cluster at the National Institutes of Health, Bethesda, MD (http://biowulf.nih.gov). *Conflict of Interest*: None declared.

References

Bianciardi M, Fukunaga M, van Gelderen P, de Zwart JA, Duyn JH. 2011. Negative BOLD-fMRI signals in large cerebral veins. J Cereb Blood Flow Metab. 31:401–412.

Cauda F, Costa T, Diano M, Sacco K, Duca S, Geminiani G, Torta DM. 2014. Massive modulation of brain areas after mechanical pain stimulation: a time-resolved fMRI study. Cereb Cortex. 24:2991–3005.

Chang C, Thomason ME, Glover GH. 2008. Mapping and correction of vascular hemodynamic latency in the BOLD signal. Neuroimage. 43:90–102.

Cohen MS. 1997. Parametric analysis of fMRI data using linear systems methods. Neuroimage. 6:93–103.

Cox RW. 1996. AFNI: software for analysis and visualization of functional magnetic resonance neuroimages. Comput Biomed Res. 29:162–173.

Devor A, Tian P, Nishimura N, Teng IC, Hillman EM, Narayanan SN, Ulbert I, Boas DA, Kleinfeld D, Dale AM. 2007. Suppressed neuronal activity and concurrent arteriolar vasoconstriction may explain negative blood oxygenation level-dependent signal. J Neurosci. 27:4452–4459.

Dosenbach NU, Visscher KM, Palmer ED, Miezin FM, Wenger KK, Kang HC, Burgund ED, Grimes AL, Schlaggar BL, Petersen SE. 2006. A core system for the implementation of task sets. Neuron. 50:799–812.

Duong TQ, Yacoub E, Adriany G, Hu X, Ugurbil K, Kim SG. 2003. Microvascular BOLD contribution at 4 and 7T in the human brain: gradient-echo and spin-echo fMRI with suppression of blood effects. Magn Reson Med. 49:1019–1027.

Friedman L, Glover GH, Krenz D, Magnotta V, First B. 2006. Reducing inter-scanner variability of activation in a multicenter fMRI study: role of smoothness equalization. Neuroimage. 32:1656–1668.

Gawryluk JR, D'Arcy RC, Mazerolle EL, Brewer KD, Beyea SD. 2011. Functional mapping in the corpus callosum: a 4T fMRI study of white matter. Neuroimage. 54:10–15.

Goense JB, Logothetis NK. 2008. Neurophysiology of the BOLD fMRI signal in awake monkeys. Curr Biol. 18:631–640.

Gonzalez-Castillo J, Saad ZS, Handwerker DA, Inati SJ, Brenowitz N, Bandettini PA. 2012. Whole-brain, time-locked activation with simple tasks revealed using massive averaging and model-free analysis. Proc Natl Acad Sci USA. 109:5487–5492.

Grootoonk S, Hutton C, Ashburner J, Howseman AM, Josephs O, Rees G, Friston KJ, Turner R. 2000. Characterization and correction of interpolation effects in the realignment of fMRI time series. Neuroimage. 11:49–57.

Handwerker DA, Ollinger JM, D'Esposito M. 2004. Variation of BOLD hemodynamic responses across subjects and brain regions and their effects on statistical analyses. Neuroimage. 21:1639–1651.

Harel N, Lee SP, Nagaoka T, Kim DS, Kim SG. 2002. Origin of negative blood oxygenation level-dependent fMRI signals. J Cereb Blood Flow Metab. 22:908–917.

Harms MP, Melcher JR. 2003. Detection and quantification of a wide range of fMRI temporal responses using a physiologically-motivated basis set. Hum Brain Mapp. 20:168–183.

Huettel SA, McCarthy G. 2001. The effects of single-trial averaging upon the spatial extent of fMRI activation. Neuroreport. 12:2411–2416.

Lieberman MD, Cunningham WA. 2009. Type I and Type II error concerns in fMRI research: re-balancing the scale. Soc Cogn Affect Neurosci. 4:423–428.

Logothetis NK. 2008. What we can do and what we cannot do with fMRI. Nature. 453:869–878.

Manson SC, Wegner C, Filippi M, Barkhof F, Beckmann C, Ciccarelli O, De Stefano N, Enzinger C, Fazekas F, Agosta F et al. 2008. Impairment of movement-associated brain deactivation in multiple sclerosis: further evidence for a functional pathology of interhemispheric neuronal inhibition. Exp Brain Res. 187:25–31.

Marxen M, Cassidy RJ, Dawson TL, Ross B, Graham SJ. 2012. Transient and sustained components of the sensorimotor BOLD response in fMRI. Magn Reson Imaging. 30:837–847.

Mazerolle EL, D'Arcy RC, Beyea SD. 2008. Detecting functional magnetic resonance imaging activation in white matter: interhemispheric transfer across the corpus callosum. BMC Neurosci. 9:84.

Newton AT, Rogers BP, Gore JC, Morgan VL. 2012. Improving measurement of functional connectivity through decreasing partial volume effects at 7T. Neuroimage. 59:2511–2517.

Orban P, Doyon J, Petrides M, Mennes M, Hoge R, Bellec P. 2015. The richness of task-evoked hemodynamic responses defines a pseudo-hierarchy of functionally meaningful brain networks. Cereb Cortex. 25:2658–2669.

Petersen SE, Dubis JW. 2012. The mixed block/event-related design. Neuroimage. 62:1177–1184.

Rostrup E, Law I, Blinkenberg M, Larsson HB, Born AP, Holm S, Paulson OB. 2000. Regional differences in the CBF and BOLD responses to hypercapnia: a combined PET and fMRI study. Neuroimage. 11:87–97.

Saad ZS, Ropella KM, Cox RW, DeYoe EA. 2001. Analysis and use of FMRI response delays. Hum Brain Mapp. 13:74–93.

Saad ZS, Ropella KM, DeYoe EA, Bandettini PA. 2003. The spatial extent of the BOLD response. Neuroimage. 19:132–144.

Sauseng P, Klimesch W, Stadler W, Schabus M, Doppelmayr M, Hanslmayr S, Gruber WR, Birbaumer N. 2005. A shift of visual spatial attention is selectively associated with human EEG alpha activity. Eur J Neurosci. 22:2917–2926.

Shmuel A, Augath M, Oeltermann A, Logothetis NK. 2006. Negative functional MRI response correlates with decreases in neuronal activity in monkey visual area V1. Nat Neurosci. 9:569–577.

Shmuel A, Yacoub E, Chaimow D, Logothetis NK, Ugurbil K. 2007. Spatio-temporal point-spread function of fMRI signal in human gray matter at 7Tesla. Neuroimage. 35:539–552.

Smith SM, Fox PT, Miller KL, Glahn DC, Fox PM, Mackay CE, Filippini N, Watkins KE, Toro R, Laird AR et al. 2009. Correspondence of the brain's functional architecture during activation and rest. Proc Natl Acad Sci USA. 106:13040–13045.

Sobel N, Prabhakaran V, Zhao Z, Desmond JE, Glover GH, Sullivan EV, Gabrieli JD. 2000. Time course of odorant-induced activation in the human primary olfactory cortex. J Neurophysiol. 83:537–551.

Tatu L, Moulin T, Vuillier F, Bogousslavsky J. 2012. Arterial territories of the human brain. Front Neurol Neurosci. 30:99–110.

Tettamanti M, Paulesu E, Scifo P, Maravita A, Fazio F, Perani D, Marzi CA. 2002. Interhemispheric transmission of visuomotor information in humans: fMRI evidence. J Neurophysiol. 88:1051–1058.

Thyreau B, Schwartz Y, Thirion B, Frouin V, Loth E, Vollstadt-Klein S, Paus T, Artiges E, Conrod PJ, Schumann G et al. 2012. Very large fMRI study using the IMAGEN database: sensitivity-specificity and population effect modeling in relation to the underlying anatomy. Neuroimage. 61:295–303.

Triantafyllou C, Hoge RD, Krueger G, Wiggins CJ, Potthast A, Wiggins GC, Wald LL. 2005. Comparison of physiological noise at 1.5T, 3T and 7T and optimization of fMRI acquisition parameters. Neuroimage. 26:243–250.

Uludag K. 2008. Transient and sustained BOLD responses to sustained visual stimulation. Magn Reson Imaging. 26:863–869.

Yacoub E, Shmuel A, Pfeuffer J, Van De Moortele PF, Adriany G, Andersen P, Vaughan JT, Merkle H, Ugurbil K, Hu X. 2001. Imaging brain function in humans at 7Tesla. Magn Reson Med. 45:588–594.